The Congo Basin Zonal Overturning Circulation

Naresh NEUPANE*

*Department of Geological Sciences, Jackson School of Geosciences, The University of Texas at Austin,
Austin, Texas 78712, USA*

ABSTRACT

The Gulf of Guinea in the equatorial Atlantic is characterized by the presence of strong subsidence at certain times of the year. This subsidence appears in June and becomes well established from July to September. Since much of the West African monsoon flow originates over the Gulf, Guinean subsidence is important for determining moisture sources for the monsoon. Using reanalysis products, I contribute to a physical understanding of what causes this seasonal subsidence, and how it relates to precipitation distributions across West Africa.

There is a seasonal zonal overturning circulation above the Congo basin and the Gulf of Guinea in the ERA-Interim, ERA-40, NCEP2, and MERRA reanalyses. The up-branch is located in the Congo basin around 20°E. Mid-tropospheric easterly flows constitute the returning-branch and sinking over the Gulf of Guinea forms the down-branch, which diverges at 2°W near the surface, with winds to the east flowing eastward to complete the circulation. This circulation is driven by surface temperature differences between the eastern Gulf and Congo basin. Land temperatures remain almost uniform, around 298 K, throughout a year, but the Guinean temperatures cool rapidly from 294 K in May to about 290 K in August. These temperature changes increase the ocean/land temperature contrast, up to 8 K, and drive the circulation.

I hypothesize that when the overturning circulation is anomalously strong, the northward moisture transport and Sahelian precipitation are also strong. This hypothesis is supported by ERA-Interim and PERSIANN-CDR (Precipitation Estimation from Remotely Sensed Information using Artificial Neural Networks-Climate Data Record) data.

Key words: climate, atmospheric dynamics, monsoon

Citation: Neupane, N., 2016: The Congo basin zonal overturning circulation. *Adv. Atmos. Sci.*, **33**(6), 767–782, doi: 10.1007/s00376-015-5190-8.

1. Introduction

Past studies (Trenberth et al., 2000; Wang, 2002a, 2002b, 2005; Nicholson and Webster, 2007; Pokam et al., 2014) indicate that atmospheric subsidence exists over the equatorial Atlantic, with the strongest sinking occurring over the central and eastern equatorial Atlantic (i.e., over the Gulf of Guinea). However, the relationship between the Gulf of Guinea subsidence and local and regional climate variability over continental Africa is not yet well explored. For example, the Gulf of Guinea is known to be a primary moisture source for the West African monsoon system (Vizy and Cook, 2001; Grist and Nicholson, 2001; Fontaine et al., 2003; Cook and Vizy, 2006), hence fluctuations in subsidence may affect rainfall patterns over the adjacent African continent by altering the low-level circulation and moisture convergence. Given Africa's strong reliance on rainfall for agricultural needs, it is important to improve our understanding of any mechanism (s) that influence rainfall variations over equatorial and West Africa. The purpose of this study is to use available data to document the seasonal-scale subsidence in the Gulf of Guinea, and improve our physical understanding of the relationship between this subsidence and boreal summer rainfall in West Africa.

The low-level Guinean subsidence (Hastenrath, 2001; Cook and Vizy, 2006; Hastenrath and Polzin, 2011) is often related to the rainfall over West Africa, including the onset of monsoon (Hagos and Cook, 2007; Caniaux et al., 2011). Using reanalyses and satellite observations, Leduc-Leballeur et al. (2013) showed that increases in the Guinean subsidence are related to increases in convection over the northern Gulf of Guinea. In an observational study, Segele et al. (2009) suggested that intensification of the Guinean surface pressure is associated with abundant rainfall in northern Africa. Similarly, Nicholson and Webster (2007), using NCEP reanalysis, observed precipitation enhancement over the Sahel when the Guinean subsidence strengthened. Studies have also indicated that this subsidence inhibits deep vertical transport of moisture over the Gulf and supports poleward moisture transport by the monsoon flow (Vizy and Cook, 2001; Neupane and Cook, 2013).

The presence of a deep atmospheric meridional overturning circulation over the Atlantic, often referred to as "the At-

---

* Corresponding author: Naresh NEUPANE
  Email: nareshneupane@utexas.edu

lantic Hadley circulation", has also been revealed, and the descending branch of this circulation, whose up-branch is located over the Sahel, has been shown to be related to the Guinean subsidence. Low-level flows from the equator toward the Sahel form the lower branch, while the equatorward flows above 600 hPa form the returning branch of the circulation. This circulation becomes most active during the boreal summer (Trenberth et al., 2000; Wang, 2004; Wang, 2005). An example can be found in Wang (2002a), who used 1950–1999 NCEP reanalysis climatology and averaged tropospheric circulation profiles from 10°W to 10°E to show the subsiding branch of the Atlantic Hadley circulation. In addition, some other studies relate this subsidence to the descending branch of a shallow meridional overturning circulation that is embedded within the deep meridional overturning circulation. The shallow circulation consists of surface southerly inflows from the Guinean Gulf and the northerly returning outflows between 700 and 500 hPa from the Sahel as well (Thorncroft and Blackburn, 1999; Zhang et al., 2006; Nolan et al., 2007; Hagos and Zhang, 2010; Thorncroft et al., 2011).

The deep and shallow meridional overturning circulations, as discussed above, are affected by Coriolis acceleration. As the onshore southerly winds flow northward onto the continent, they tend to deviate eastward because of the action of zonal Coriolis acceleration. It is difficult for a purely meridional flow to be maintained. The Coriolis force appears as soon as an air parcel is deflected in a meridional direction and imparts zonal acceleration to the parcel.

The zonal circulations along the equator, e.g., Walker circulation, remain unaffected by the Coriolis acceleration. Vizy and Cook (2001) hypothesized that a Walker-type circulation exists above the Congo basin and the Gulf of Guinea. They used an AGCM forced with warm SST anomalies in the Gulf. Rainfall increased along the coast and decreased over the Congo basin when the SSTs were anomalously high, and it was found to be associated with a weakening of the circulation. This circulation can also be seen in zonal and vertical wind streamlines along the equator in Lau and Yang (2003, Fig. 2c). They used the 1949–1999 NCEP climatology for July to show the Walker circulations around the globe. In addition, sketches indicating the presence of this circulation can be seen in Hastenrath (2006) and the references therein.

A number of recent studies have indicated the existence of low-level westerly flows from the Gulf to the Congo basin. The circulation shows that the increased rainfall over the Congo basin is associated with anomalously stronger low-level westerly (LLW) flows (Pokam et al., 2012; Dezfuli and Nicholson, 2013; Nicholson and Dezfuli, 2013; Dezfuli et al., 2015); plus, the circulation is often associated with the northward flows and rainfall across West Africa, as discussed in Cook and Vizy (2015). These studies mostly focused on equatorial atmospheric circulation in the spring and fall. Pokam et al. (2014) investigated the seasonal variability and driver of the LLW flows using four reanalyses for the period 1989–2003. The LLW, driven by the land–ocean temperature contrast, forms the lower branch of the Walker-type

circulation. This is weakest in spring and strongest in fall. This also suggests that the West African monsoon system and the atmospheric circulation over eastern equatorial Atlantic are closely connected. In this study, a zonal overturning circulation is identified over the Gulf of Guinea and the Congo basin. The variability of the circulation is examined based on an index obtained from the rising branch. This index is further used to understand the relationship between the circulation and rainfall and moisture distributions across West Africa. The focus is on the West African monsoon season, from July through September, when the overturning circulation is most pronounced.

2.   Data

Since there is some degree of uncertainty in the observations, various observational and reanalysis datasets are analyzed and compared to each other to build confidence in the findings. Each dataset is discussed briefly below.

Four reanalysis datasets are utilized to provide monthly mean information regarding the circulation, temperature, and geopotential height fields: the 1.125°-resolution ERA-40 (Uppala et al., 2005); the 1.5°-resolution ERA-Interim (Dee et al., 2011); the 2.5°-resolution NCEP-2 (Kanamitsu et al., 2002); and the 1.25°-resolution MERRA (Rienecker et al., 2011). ERA-Interim, MERRA and NCEP-2 cover the same period (1979–2013), while ERA-40 has data available for the period 1958–2002. The analysis will be conducted over the full available period.

The number of vertical levels differs among the reanalyses, ranging from 17 levels in NCEP-2, 23 levels in ERA-40, 37 levels in ERA-Interim, and 42 levels in MERRA. Analysis will focus on comparing standard levels among the different reanalyses. Also, the 2.5°-resolution NOAA OLR data are used (Liebmann and Smith, 1996). The reanalysis is available for the period 1974–2013.

Precipitation estimates from two datasets are used: the 0.25°-resolution NASA TRMM satellite-derived monthly rainfall product for the period 1998–2013 (TRMM 3B42V7; Kummerow et al., 1998), and version 1 of the 0.25°-resolution PERSIANN-CDR (Precipitation Estimation from Remotely Sensed Information using Artificial Neural Networks-Climate Data Record) dataset (Sorooshian et al., 2000) for the period 1983–2013. The 0.5°-resolution CRU gridded monthly surface temperature dataset (CRUTS3.21; Mitchell and Jones, 2005) is also used. This dataset provides land-based monthly rainfall and surface temperature estimates for the period 1901–2012.

3.   Results

3.1.   *Identification of the Congo basin zonal overturning circulation*

Figure 1 shows the ERA-Interim 1979–2013 climatological vertical p-velocity [i.e., omega, $\omega \times 10^{-2}$ (Pa s^{-1})] at 900 hPa for the January–February–March (JFM, Fig. 1a), April–
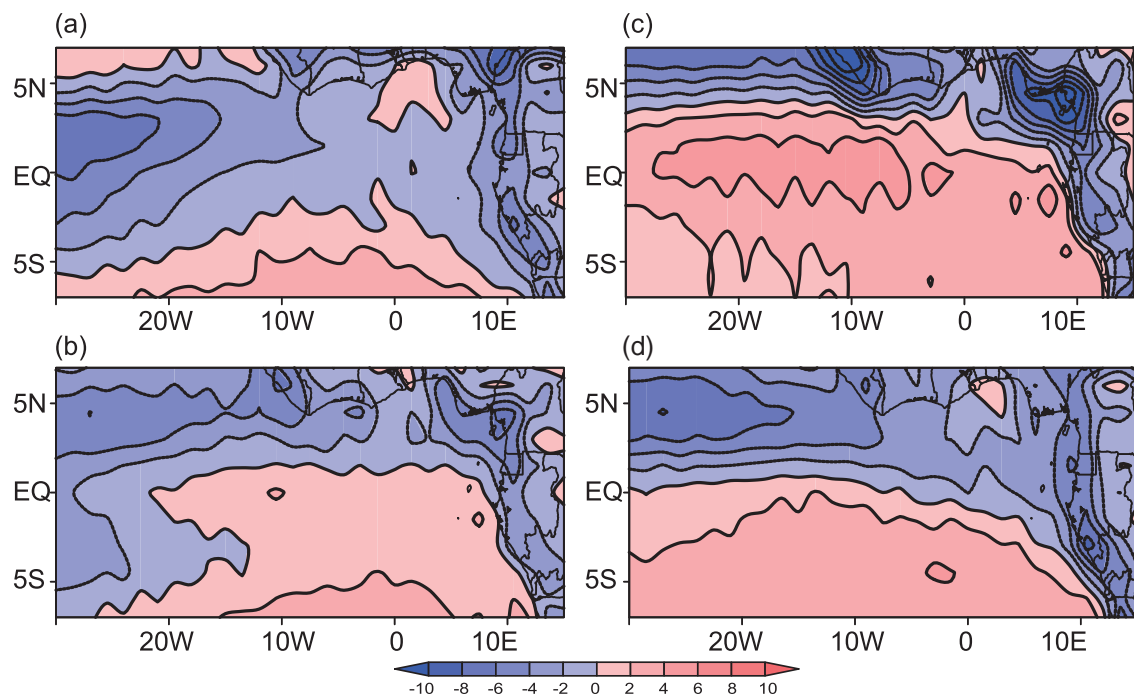
Fig. 1. ERA-Interim climatological monthly 900-hPa p-velocity (omega; $\times 10^2$ Pa s^{-1}) for the (a) JFM, (b) AMJ, (c) JAS and (d) OND means. Positive values indicate sinking motion.

May–June (AMJ, Fig. 1b), July–August–September (JAS, Fig. 1c), and October–November–December (OND, Fig. 1d) means. In JFM, there is rising motion along the equatorial Atlantic (Fig. 1a). In AMJ, this rising is replaced with sinking motion, up to 4×10^{-2} Pa s^{-1}, over the central equatorial Atlantic (7°–25°W) and the Gulf of Guinea near 8°E, clearly distinguishable from the central Atlantic maxima (Fig. 1b). In JAS, both the central Atlantic and Gulf of Guinea subsidence maxima expand in spatial extent, with the latter extending from 4°E to 10°E between 5°S and 3°N (Fig. 1c). The Guinean subsidence maximum reaches its peak strength of approximately 8×10^{-2} Pa s^{-1}, e.g., near (1°S, 8°E), and subsidence near 0°E extends northward up to 4°N. The maximum over the central equatorial Atlantic remains robust in size, but aloof from the Guinean maximum—for example, at (0°, 8°E). This subsidence becomes sufficiently weak in winter, and is replaced with rising motion, up to -6×10^{-2} Pa s^{-1} (OND, Fig. 1d). Over land, rising vertical motions occur year round.

It is clear from Fig. 1 that boreal summer is associated with subsidence over the equatorial Atlantic between 5°S and 3°N, with two centers of maximum intensity—one over the central Atlantic (Wang, 2004) and the other over the Gulf of Guinea in the eastern Atlantic. Sinking motion maximizes over both regions in summer (Fig. 1c). The Guinean subsidence exhibits a distinct seasonal cycle (not shown). The subsidence is primarily located to the south of the equator from January through May. In June, it appears over the Gulf of Guinea and starts its northward progression, maximizes and reaches its northernmost location of around 5°N from July to September, and then weakens and retreats south of the equator by October. ERA-40, NCEP-2 and MERRA exhibit

a similar seasonal cycle (not shown).

Figure 2 shows the longitude–height cross section of zonal and vertical p-velocity wind components [u (m s^{-1}); $\omega \times 10^{-2}$ (Pa s^{-1})] averaged between 5°S and 3°N from the ERA-Interim climatology (1979–2013) for the JFM (Fig. 2a), AMJ (Fig. 2b), JAS (Fig. 2c) and OND (Fig. 2d) means. In JFM, there is rising motion, as indicated by the upward-pointing streamlines in the Gulf of Guinea (centered around 10°E; Fig. 2a). Compared with the JFM mean, rising motion becomes weaker in AMJ (Fig. 2b). In JAS (Fig. 2c), there is a circulation near the surface between 2°W and 30°E, with rising motions from the surface to 650 hPa over the Congo basin from 12°E to 25°E, westward flow around 800 hPa from 15°E to 2°W, and subsidence along the equatorial West African coast at 2°W. Westerly onshore flow from the Gulf of Guinea into the Congo basin is shallow, generally confined to between the surface and 850 hPa, extending inland to about 12°E. The vertical extent of the circulation appears to be predominantly confined to the boundary layer (i.e., the surface to 800 hPa), with evidence of some mid-tropospheric (i.e., 700–400 hPa) rising (sinking) motion east (west) of 10°E. This circulation is identified as the Congo basin zonal overturning circulation. The circulation contracts in size and it almost disappears in OND (Fig. 2d), although the rising branch remains strong over the Congo during this time (Fig. 2d). This seasonality is also depicted in ERA-40, NCEP-2, MERRA, and JRA (1958–2014; not shown).

A comparison of Figs. 1 and 2 indicates that the seasonality of the Guinean subsidence east of 2°W and the Congo basin overturning circulation behave in a similar manner, especially during the boreal summer months of June to October, with the subsidence and Walker-type circulation's strength
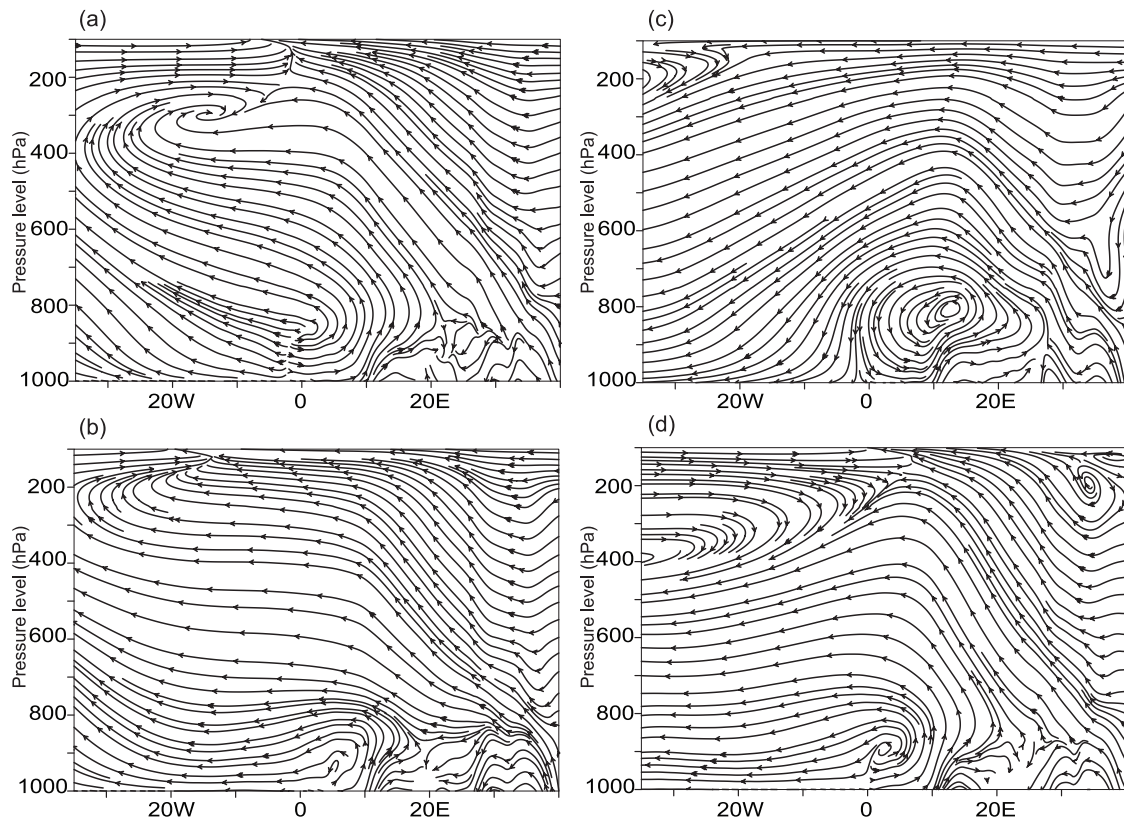
Fig. 2. ERA-Interim climatological monthly longitude–height cross section of streamlines [u (m s^{-1}); $-\omega \times 10^2$ (Pa s^{-1})] averaged over 5°S–3°N for the (a) JFM, (b) AMJ, (c) JAS, and (d) OND means.

being strongest from July to September. Thus, the rest of the analysis presented below will focus on physically understanding the maintenance of the Congo basin zonal overturning circulation and its relationship to subsidence over the Gulf of Guinea for the July–September period. Figures 3a–d show climatological July–September vertical cross sections of the zonal–omega wind components (vectors), and the meridional wind component (contours), averaged from 5°S to 3°N for ERA-Interim, ERA-40, NCEP-2 and MERRA. All of the reanalyses show Walker-type circulation with rising motions over the Congo basin centered at 20°E and extending from near the surface to the upper troposphere, easterly flow around 650 hPa between 0°E and 20°E, and subsidence over the Gulf of Guinea that diverges at 2°W near the surface. Below 800 hPa from 2°W to 25°E, the flow is predominantly westerly, constituting the lower onshore branch of the circulation. Note that near the surface over this region there is also a southerly component to the flow, but it is generally weaker in magnitude (e.g., up to 3 m s^{-1} in ERA-Interim). The circulation is embedded within a large-scale incomplete circulation that rises over the Congo basin, flows westward above 600 hPa, subsides over the Atlantic, but lacks the lower branch to complete the circulation.

While the basic structure of the Congo basin zonal overturning circulation is captured by all of the reanalyses, there are still some differences among the datasets. For instance, the rising branch is stronger in ERA-Interim and ERA-40

than in NCEP-2 and MERRA. At 15°E and 700 hPa, the upward p-velocity is around 4×10^{-2} Pa s^{-1} in ERA-Interim, ERA-40 and NCEP-2, while it is replaced with a downward p-velocity of about -1×10^{-2} Pa s^{-1} in MERRA.

Based upon Figs. 2 and 3, the boundaries of the Congo basin zonal overturning circulation during July–September can be defined. The up-branch is located within (5°S–3°N, 15°–25°E) over the Congo basin, while the down-branch is within (5°S–3°N, 2°W–8°E) over the Gulf of Guinea. Therefore, unless mentioned, the Gulf of Guinea and Congo basin regions in this paper are (5°S–3°N, 2°W–8°E) and (5°S–3°N, 15°–25°E), respectively. The 650 hPa easterly and the surface westerly constitute the up-branch and lower-branch (Figs. 3a–d).

The idea of there being a Walker-type circulation is not a new concept; previous studies have suggested the possibility of such a circulation (Vizy and Cook, 2001; Lau and Yang, 2003; Hastenrath, 2006). Pokam et al. (2014) reported the presence of this circulation. The lower branch is driven by the land–ocean heating contrast, and it develops well from September to November. As stated in the introduction, the focus here is on the West African monsoon season, July–September.

The lower branch of the circulation is explored. Figures 4a–d display the July–September climatological 925-hPa geopotential heights and winds from ERA-Interim, ERA-40, NCEP-2 and MERRA, respectively. Heights are high
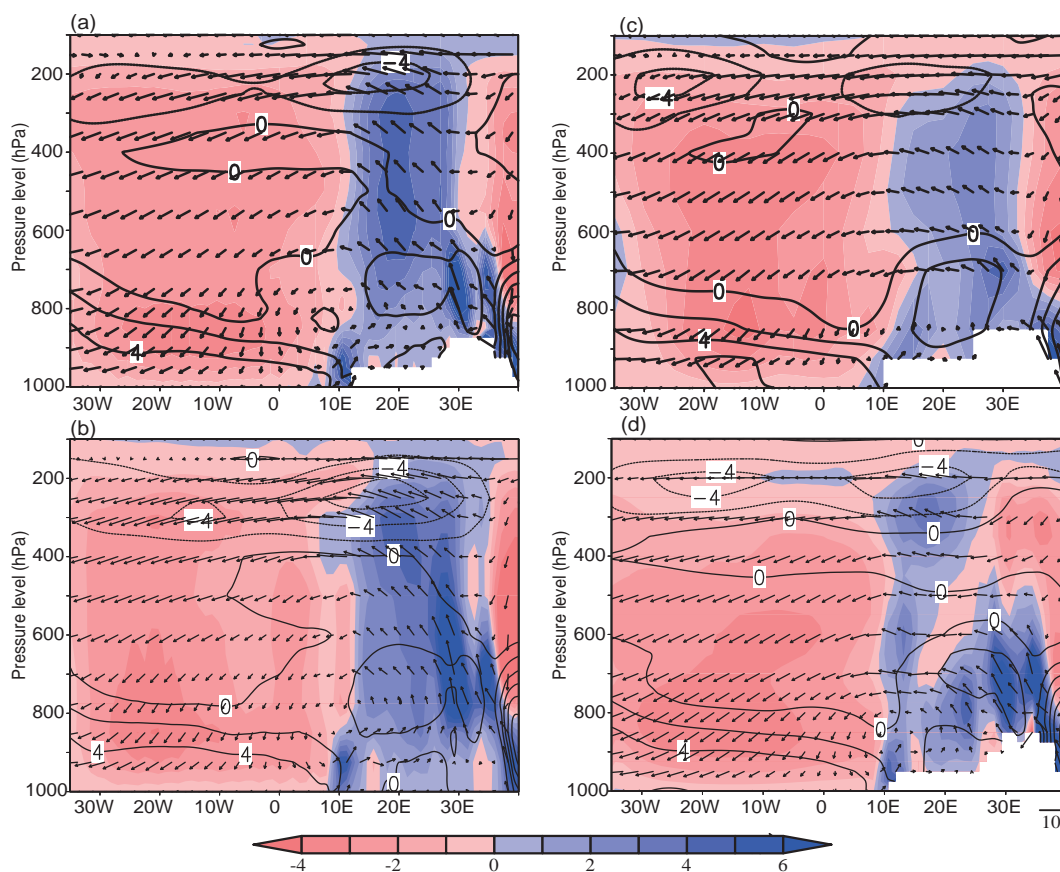
Fig. 3. Vertical cross section of zonal vertical p-velocity [u (m s^{-1}); $-\omega \times 10^2$ (Pa s^{-1}); vectors], vertical p-velocity [$-\omega \times 10^2$ (Pa s^{-1}); shading] and meridional winds [v (m s^{-1}); contours] averaged over 5°S–3°N for the JAS mean from (a) ERA-Interim, (b) ERA-40, (c) NCEP-2 and (d) MERRA climatologies. Blue shading indicates upward motion. Values under the topography are masked white in (a), (c), and (d).
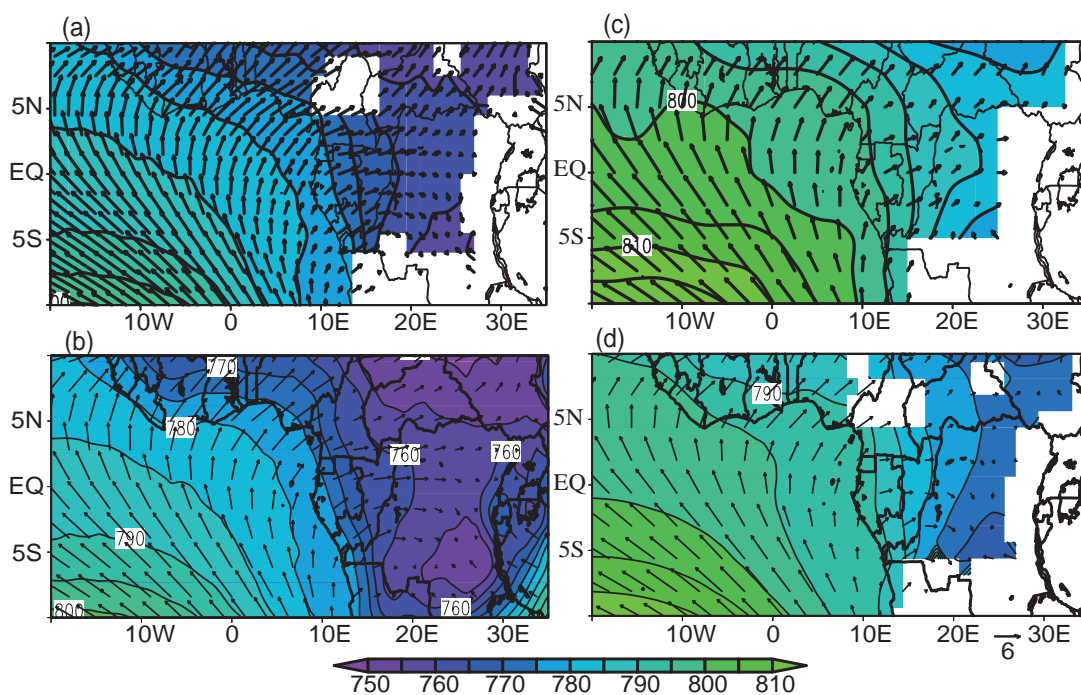
Fig. 4. JAS climatological 925-hPa geopotential heights (shading; gpm) and winds (vector; m s^{-1}) from (a) ERA-Interim, (b) ERA-40, (c) NCEP-2 and (d) MERRA. Values under the topography are masked white in (a), (c), and (d).

over the equatorial Atlantic and low over the Congo basin, associated with the zonal height gradient between the Gulf of Guinea and the Congo basin (e.g., heights approximately 20 gpm lower over the Congo basin than the Gulf of Guinea). Associated with this zonal gradient is predominantly westerly flow in the vicinity of the equator from about 10°E to 25°E, and the zonal flow is stronger than the meridional flow. For example, westerly wind reaches up to 6 m s^{-1}, whereas southerly wind reaches up to 2 m s^{-1}. Also, as shown in Fig. 3, the southerly flow is much weaker than the westerly flow in the region of interest from the surface to 800 hPa. These zonal flows remain undeflected by the Coriolis force. For these reasons, and also as discussed in the introduction, the focus here is on zonal circulation.

To understand the maintenance of the zonal overturning circulation, the geopotential height gradient and its relationship with the low-level circulation, the horizontal momentum equations are analyzed. The zonal (i.e., u-) and meridional (i.e., v-) components of the equation are as follows:

$$\frac{du}{dt} = -\frac{\partial \Phi}{\partial x} + fv + R_x, \qquad (1)$$

and

$$\frac{du}{dt} = -\frac{\partial \Phi}{\partial y} - fu + R_y, \qquad (2)$$

where u is the zonal wind and v is the meridional wind. In Eq. (1) [Eq. (2)], the total zonal (meridional) acceleration is balanced on the right-hand side by the acceleration due to the zonal (meridional) pressure gradient $-(\partial \Phi / \partial x)[-(\partial \Phi /$ $\partial y)]$, where Φ is geopotential, the Coriolis acceleration component [for which $f \equiv 2\Omega \sin \phi$ is the Coriolis parameter, where Ω is the angular speed of the rotation of Earth ($=$ 7.3×10^{-5} rad s^{-1}) and ϕ is latitude], and the zonal (meridional) frictional acceleration, represented by the terms R_x (R_y). Six-hourly values are used to calculate the daily and monthly values of the variables in the above equations. The acceleration term (Lagrangian acceleration) on the left is calculated as the sum of the Eulerian and convective accelerations. Note that R_x and R_y are calculated as residuals in the analysis, and therefore may contain errors due to the estimation of derivatives by finite differencing.

Figure 5 shows the 925-hPa July–September climatological value of each term in the horizontal momentum equations [Eqs. (1) and (2)] from ERA-Interim, ERA-40, NCEP-2 and MERRA. Close to the equator, the total acceleration (top row) is small. Likewise, at the equator, the acceleration associated with the Coriolis force (third row) is small as f approaches zero. Thus, the primary balance occurs between the acceleration associated with the pressure gradient (second row) and the residual/friction term (fourth row). The pressure gradient force is primarily eastward over equatorial Africa, with the strongest magnitudes occurring between 12°E and 18°E in the Congo basin. In contrast, over the equatorial Atlantic, the pressure gradient acceleration is much weaker. Values are greater over coastal inland areas than over the ocean. For example, in ERA-Interim (Fig. 5b), it is about 6×10^{-5} m s^{-2} over the equatorial Gulf of Guinea, while it is 18×10^{-5} m s^{-2} over the Congo basin. For the most part, the acceleration
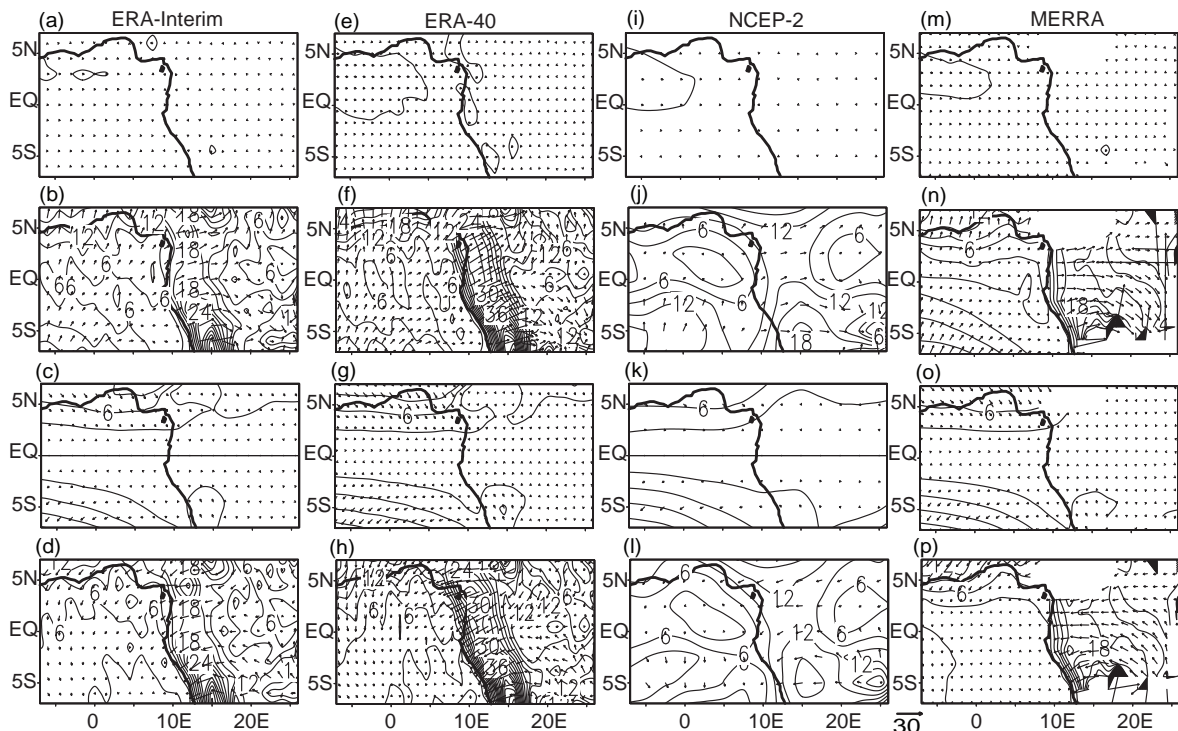

Fig. 5. Vectors showing combinations of terms in Eqs. (1) and (2), with contours displaying magnitudes (10^{-5} m s^{-2}) at 925 hPa for the JAS mean, as follows: total acceleration (first row); acceleration associated with the geopotential height gradient (second row); acceleration associated with the Coriolis force (third row); and residual terms (fourth row).

associated with the residual/friction term opposes the wind direction (Fig. 4), and has larger magnitude over land with complex topography, such as over western equatorial Africa. This shows that, associated with the friction due to topography, there is convergence of winds over the Congo basin.

In general, the 925-hPa geopotential heights are much lower in the Congo basin than in the Gulf of Guinea and, associated with this gradient, the flow is directed eastward and there is strong convergence over the Congo basin (Figs. 4 and 5). Investigation of the underlying surface temperature distributions helps to understand the low-level geopotential height differences between the Congo basin and the Gulf. Figure 6 shows the climatological July–September surface temperatures for ERA-Interim (Fig. 6a), ERA-40 (Fig. 6b), NCEP-2 (Fig. 6c) and MERRA (Fig. 6d), as well as the CRUTS.3.21 1901–2012 observational dataset (Fig. 6e). Over the tropical eastern Atlantic, a cold tongue of relatively cooler SSTs forms, beginning in the late spring and reaching a minimum by late summer (Hastenrath and Lamb, 2004). This feature is represented in all of the reanalyses shown in Fig. 6 by the area of relatively cooler temperatures of 296 K between 5°S and the equator spanning from 10°W to the African coast. North of the equator, Atlantic SSTs are slightly warmer (i.e., up to 298–299 K). Generally, all of the reanalyses exhibit similar SST distributions over the Atlantic, which is not surprising since these datasets are typically forced with the observed SSTs. Over continental Africa, surface temperatures vary among the datasets, attributable to the different land surface models included in predicting them. For example, compared with the observed CRUTS3.21 surface temperatures,

the Congo basin temperatures are about 2 K cooler in ERA-Interim, ERA-40 and NCEP-2, while around 4 K warmer in MERRA (Fig. 6e). Despite these differences, the reanalyses generally indicate the existence of a surface temperature difference near the equator between the relatively cooler Gulf of Guinea and the relatively warmer Congo basin.

Next, climatological monthly 925-hPa temperatures are area-averaged over the Gulf of Guinea (5°S–3°N, 2°W–8°E) and the Congo basin (5°S–3°N, 15°–25°E) and compared to one another for each reanalysis. Figure 7a shows the monthly Congo basin (long-dashed line) and the Gulf of Guinea (short-dashed line) surface temperatures, and the differences in the Congo basin and the Gulf of Guinea temperatures are shown in Fig. 7b. Note that it is chosen to conduct this evaluation at 925 hPa to reduce the impact that differences in surface elevation may have on the comparison.

The results in Fig. 7a indicate that all of the reanalyses generally agree that the Congo basin 925-hPa temperatures are warmer than those of the Gulf of Guinea for all months. Furthermore, the seasonal variability over the annual cycle is much less over the Congo basin compared to the Gulf of Guinea, as temperatures generally fluctuate by 2 K or less for the former compared to around 5–6 K for the latter.

In terms of the Congo basin and Gulf of Guinea temperature difference, it is positive year round, but relatively small (i.e., 3 K or less) from November to April for three of the four reanalyses (Fig. 7b). The exception, MERRA, has differences between 4 and 5.5 K during November–April. During the boreal summer months, the differences increase in May and June, peaking in July and August (at around 5 K in ERA-
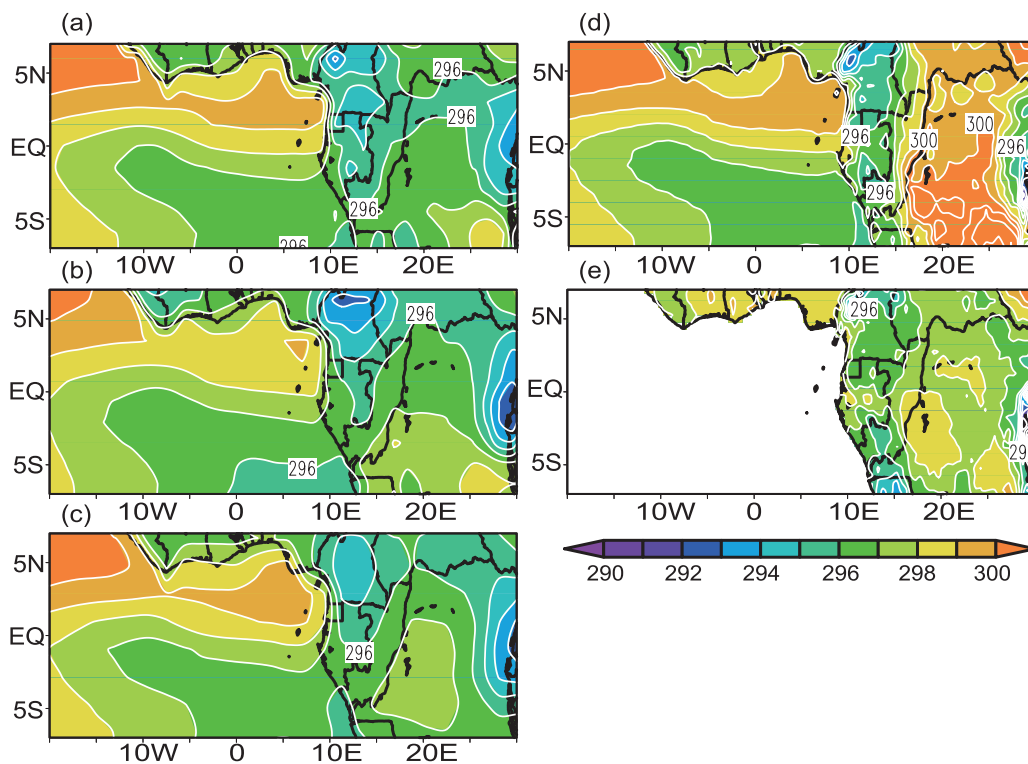

Fig. 6. Climatological JAS surface temperatures (K) from (a) ERA-Interim, (b) ERA-40, (c) NCEP-2 and (d) MERRA, as well as from (e) CRUTS3.21 observations. Contour interval: 1 K.
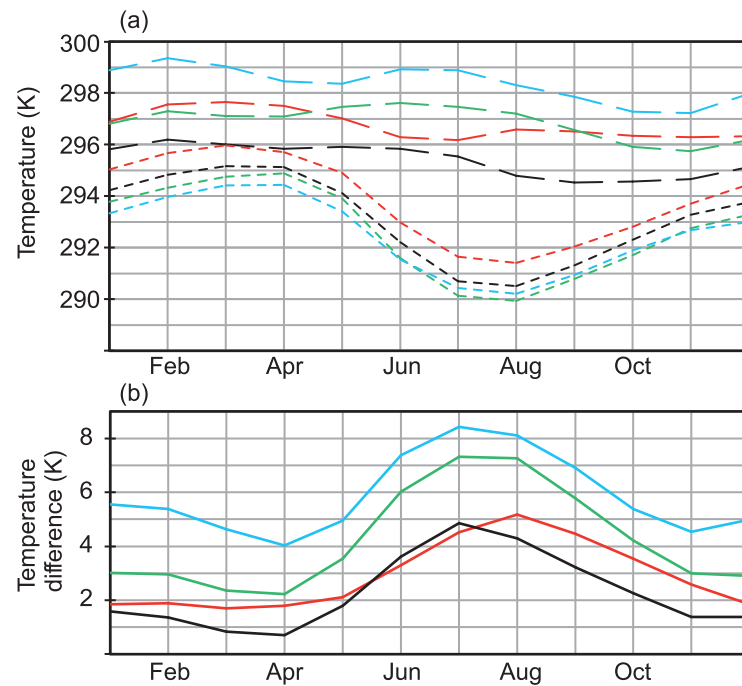
Fig. 7. (a) 925-hPa climatological monthly mean temperatures (K) in the Congo basin (5°S–3°N, 15°–25°E; long-dashed lines) and the Gulf of Guinea (5°S–3°N, 2°W–8°E; short-dashed lines) from ERA-Interim (black), ERA-40 (green), NCEP-2 (red) and MERRA (blue). (b) 925-hPa climatological monthly mean temperature differences (K) between the Congo basin and the Gulf of Guinea from ERA-Interim (black), ERA-40 (green), NCEP-2 (red) and MERRA (blue).

Interim and NCEP-2, 7.3 K in ERA-40, and above 8 K in MERRA), and then after August the difference begins to decrease as the cold upwelling weakens in the Gulf of Guinea. It is this low-level temperature difference that drives the overturning circulation. The circulation appears when the temperature difference starts increasing in June, becomes well developed from July to September when the temperature difference is largest, and, as the eastern equatorial Atlantic cold tongue weakens, the circulation starts weakening and disappears in the fall (Figs. 2 and 7).

These results suggest that it is important to have an accurate representation of the Congo basin/Gulf of Guinea low-level temperature gradient associated with the zonal circulation. Guinean temperatures are similar in the reanalyses; therefore, gradient differences are largely determined by the Congo basin temperatures. Many potential factors can influence the low-level temperatures over land, which can result in the inter-reanalysis spread shown in Fig. 7. One of the important factors is how each reanalysis treats the prediction of land surface conditions; however, understanding this is better left to the individual reanalysis groups, as they will have a better understanding of the intricacies of their respective reanalysis modeling algorithms. A more basic factor is to evaluate the precipitation in the different reanalyses, since temperature and precipitation are tightly related. For this reason, precipitation in the reanalyses are examined next.

Climatological July–September precipitation rates are

shown in Fig. 8 for the TRMM (Fig. 8a) and PERSIANN (Fig. 8b) observations, as well as for ERA-Interim (Fig. 8c), ERA-40 (Fig. 8d), NCEP-2 (Fig. 8e) and MERRA (Fig. 8f). TRMM and PERSIANN indicate a zonally oriented band of precipitation across Africa during July–September, with maxima centered at (2°N, 18°W) and (5°N, 8°E) over the Cameroon highlands (Figs. 8a and b). Rainfall rates over the northern Democratic Republic of Congo (DRC) are over 7 mm d^{-1} and gradually decrease to about 3 mm d^{-1} around 5°S.

The zonally elongated band of rainfall with the two maxima is represented in each reanalysis (Figs. 8c–f), albeit the magnitudes of the maxima vary among the different-resolution datasets. Over the DRC, there are differences in the rainfall distributions among the reanalyses, with MERRA, ERA-40 and NCEP-2 demonstrating considerably drier results than TRMM. Of the four reanalyses, ERA-Interim captures the July–September distribution of rainfall over the DRC most realistically.

Next, the 600-hPa winds and temperature are examined (figures not shown). The flow is primarily easterly from the Congo basin to the Gulf of Guinea near the equator, and this easterly flow constitutes the returning branch of the overturning circulation. Similar to the lower branch, this branch is driven by the temperature gradient. The Gulf of Guinea is warmer than the Congo basin. The difference is positive, up to 0.06 K in ERA-Interim, 0.27 K in ERA-40, 0.3 K in
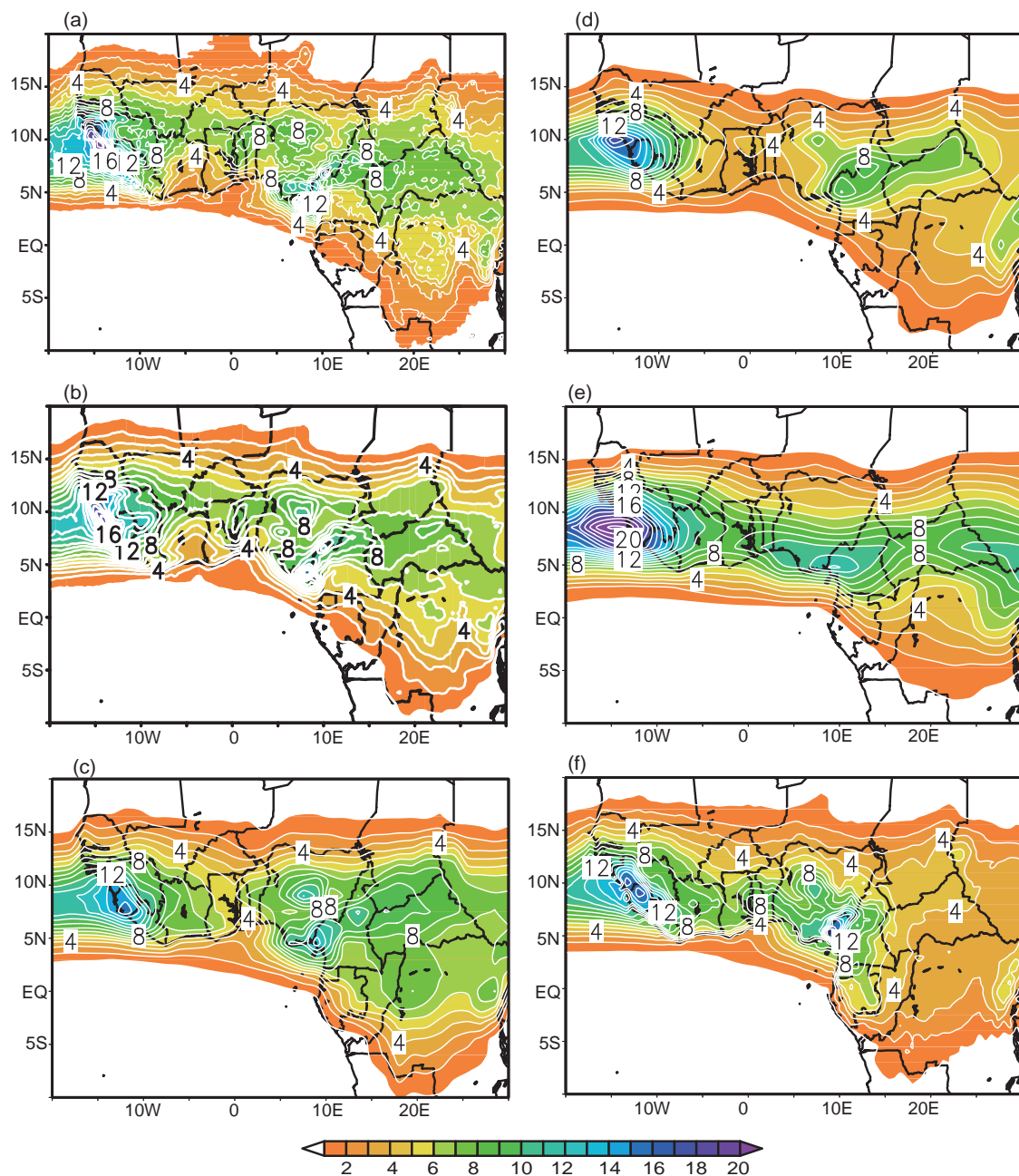
Fig. 8. Climatological JAS precipitation rates (mm d^{-1}) from (a) TRMM 3B42V7 satellite derived rainfall estimates, (b) PERSIANN-CDR precipitation estimates, and the four reanalysis datasets [(c) ERA-Interim; (d) ERA-40; (e) NCEP-2; (f) MERRA].

NCEP-2, and 0.35 K in MERRA. Exploring the relationship between the upper branch of this equatorial overturning circulation along the equator and the African easterly jet located further north in the Sahel is beyond the scope of this study.

3.2. *Relationship between the Congo basin zonal overturning circulation and West African atmospheric circulation*

There are differences in the representation of ocean–land temperature gradient in the reanalyses. For example, during the summer, temperature differences vary from 5 to 8

K among the reanalyses. These gradient differences are associated with variations in representing land temperature, as discussed above (Fig. 7). Since land temperature is closely tied with precipitation, the precipitation values in the reanalyses are investigated. Compared to the other three reanalyses (MERRA, ERA-40 and NCEP-2), ERA-Interim accurately represents the precipitation values (Fig. 8). This is consistent with the findings of Simmons et al. (2010), who also reported that the precipitation field is generally better represented in ERA-Interim compared with ERA-40. Also, in representing the Congo basin precipitation, large differences

exist among datasets and models, as shown by Washington et al. (2013). In total, including the spring, which was the focus of their analysis, ERA-Interim and ERA-40 yield wetter results than the NCEP reanalysis. Lower summertime rainfall rates (for example in MERRA) are likely associated with increased surface heating due to a lack of convection, warmer-than-observed surface temperatures predicted over the DRC (e.g., Fig. 6b), and hence a larger low-level Congo basin–Gulf of Guinea temperature contrast (Fig. 7b). Since ERA-Interim provides the most realistic representation of climatological July–September surface temperature and precipitation fields, as reported in section 3.1 (Figs. 6 and 8), this reanalysis is used to examine the relationship. I hypothesize that, when the rising branch of the circulation is strong, the northward moisture transport and rainfall becomes strong across West Africa, including the Sahel.

Monthly omega wind anomalies for July–September from 1979 to 2013 are calculated by subtracting the 1979–2013 climatological mean. Doing so removes the seasonal cycle from the time series to foster a better comparison over different months. From the above anomalies field, an 800-hPa area-average index is created. The area used is (5°S–3°N, 15°–25°E). This area corresponds to the rising branch of the overturning circulation, discussed earlier in section 3.1 (Fig. 2), while 800 hPa is chosen to be sufficiently above the topography of the region. The black box shown in Fig. 9 denotes the averaging region.

Figure 9 shows the correlation coefficients (multiplied by 100) between the Congo basin index and the July–September p-velocity field at 850 hPa for ERA-Interim. The 850-hPa level is selected because the Guinean subsidence is much larger at this level (see Fig. 3a). Correlations are negative, up to 50% (significant at the 5% level), in the equatorial Atlantic (5°S–3°N, 25°W–7°E), including the Gulf of Guinea. This implies that, when the rising motions over the Congo basin become stronger, subsidence over the Gulf of Guinea becomes strong, and vice versa. North of the equator, significant positive correlations are centered along 10°N over West Africa and southern Chad. This suggests that stronger rising motion over the Congo basin is also associated with stronger rising motion in the Sahel. The Guinean index (5°S–3°N, 2°W–8°E) shows much stronger positive correlations (up to 100%) in the Gulf and negative correlations in the Congo basin, lending further support to the existence of a relationship between the Guinean subsidence and the Congo basin rising, as discussed above (figure not shown).

Figure 10a shows the time series of the 800-hPa vertical p-velocity index for JAS only from ERA-Interim. We investigate the physics of this variability. A negative value indicates a stronger rising motion. The index is mainly negative from 1979 to 1994. In 1995, there is an abrupt shift and the index is found to be primarily positive after 1994. For example, from 1979 to 1994, 37 of the total 48 JAS periods are negative; while from 1995 to 2013, 49 of the total 57 are positive. This discontinuity is likely associated with various adjustments made to the ERA-Interim algorithm (e.g., new bias correction schemes, new moisture analysis and model physics schemes
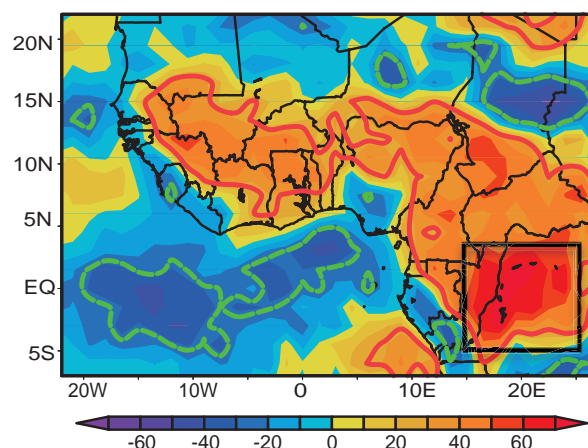

Fig. 9. Correlation coefficients (multiplied by 100) between the ERA-Interim 800-hPa Congo basin p-velocity index and the vertical p-velocity for JAS. Correlation coefficients exceeding the 95% confidence level are enclosed within red and green-dashed lines. Region (5°S–3°N, 15°–25°E) indicates the Congo basin.

have been used to maintain consistency among observing systems) and data input (Simmons et al., 2007; Uppala et al., 2008; Dee and Uppala, 2009; Kobayashi et al., 2009).

To remove this shift, the time series is divided into two parts (1979–1994 and 1995–2013), and each part of the time series is scaled with its own climatology. For example, the 1979–1994 July climatology is subtracted from the 16 months of July during 1979–1994 to obtain the deseasonalised value for July, with August and September created in a similar manner. Likewise, the 1995–2013 JAS periods are similarly produced, but by utilizing the 1995–2013 climatology for the appropriate month.

Figure 10b shows the adjusted Congo basin index. The dashed lines correspond to ±1 standard deviation. Positive and negative index values are now more evenly distributed over the time series and there is no longer any evidence of a discontinuity in 1995. The index shown in Fig. 10b is used to detect individual months when the Congo basin vertical p-velocity index is strong and weak for JAS, and hence identify particular months when the circulation is strong or weak. A strong circulation month is defined as when the index value is less than -0.6×10^{-2} Pa s^{-1}, which corresponds to -1 standard deviation from the mean; whereas, a weak circulation month is defined as when the index is greater than $+0.6 \times 10^{-2}$ Pa s^{-1}, which corresponds to $+1$ standard deviation from the mean. Table 1 shows the months identified for each case. This index represents the zonal overturning circulation.

Figures 11a–c show the JAS vertical cross sections of the zonal and vertical components of the wind (streamlines) and vertical winds (shaded) averaged from 5°S to 3°N for the reanalysis climatology (Fig. 11a), as well as the weak (Fig. 11b) and strong (Fig. 11c) circulation composites. In the climatology, the circulation extends from the surface to 700 hPa, where the upward p-velocity is about 5×10^{-2} Pa s^{-1}
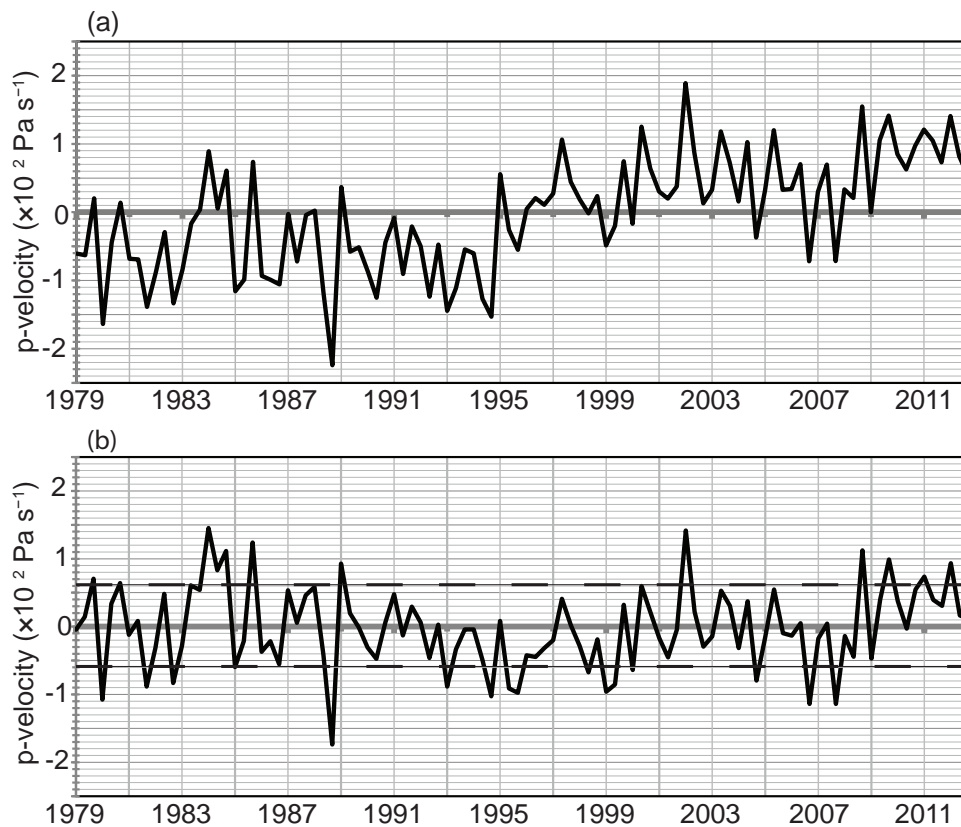
Fig. 10. (a) 800-hPa average (5°S–3°N, 15°–25°E) vertical p-velocity ($\times 10^2$ Pa s^{-1}) differences in JAS and their climatologies from ERA-Interim (1979–2013). (b) As in (a) but the vertical p-velocity values before 1994 are subtracted from the 1979–94 mean, and the values after 1995 are subtracted from the 1995–2013 mean. The dashed lines in (b) indicate ± 1 standard deviation.

Table 1. Summary of weak and strong Congo basin Walker circulation months.

	Weak	Strong
1.	September 1979	July 1980
2.	September 1980	September 1981
3.	August 1983	September 1982
4.	July 1984	September 1988
5.	August 1984	July 1993
6.	September 1984	September 1994
7.	September 1985	August 1995
8.	July 1989	September 1995
9.	August 2000	August 1998
10.	July 2002	July 1999
11.	September 2008	August 1999
12.	September 2009	July 2000
13.	September 2010	July 2001
14.	July 2011	September 2004
15.	July 2012	September 2006
16.		September 2007

(Fig. 11a). In the weak composite, the rising branch weakens; for example, the rising motion at (15°E, 800 hPa) is about 2×10^{-2} Pa s^{-1} weaker than in the climatology (Fig. 11b). In contrast, upward vertical motions are stronger than in the climatology, by up to 2×10^{-2} Pa s^{-1}, in the strong circula-

tion composite case (Fig. 11c). The sinking in the Gulf and rising in the Congo basin in the strong composite is significantly different (at the 95% confidence level) from the weak composite (not shown), meaning that a strong circulation case is different from a weak circulation case.

The relationship between the overturning equatorial circulation and regional-scale circulation and rainfall in West Africa is explored by analyzing the low-level circulation and moisture fields in Figs. 11d–f. Figure 11d shows the climatological 800-hPa geopotential heights and moisture transport vectors for the JAS climatology. The 800-hPa level is selected for consistency with the level used to create the two composite cases, as discussed earlier. Associated with the North Atlantic subtropical high, the largest heights are located off the coast of West Africa. The smallest height is located over the continent, east of 15°E. Moisture transport is predominantly westerly–southwesterly over the Guinean coast and coastal inland areas (0°–7°N, 0°–15°E). Transport vectors are primarily easterly to the south of the equator.

Figure 11e displays the 800-hPa geopotential heights and moisture transport differences in the weak composite and the climatology, and the differences in the strong composite and climatology are shown in Fig. 11f. Geopotential heights are larger, up to 2 gpm, in the weak composite than in the climatology in the Sahel (10°–20°N, 25°W–20°E), and the heights
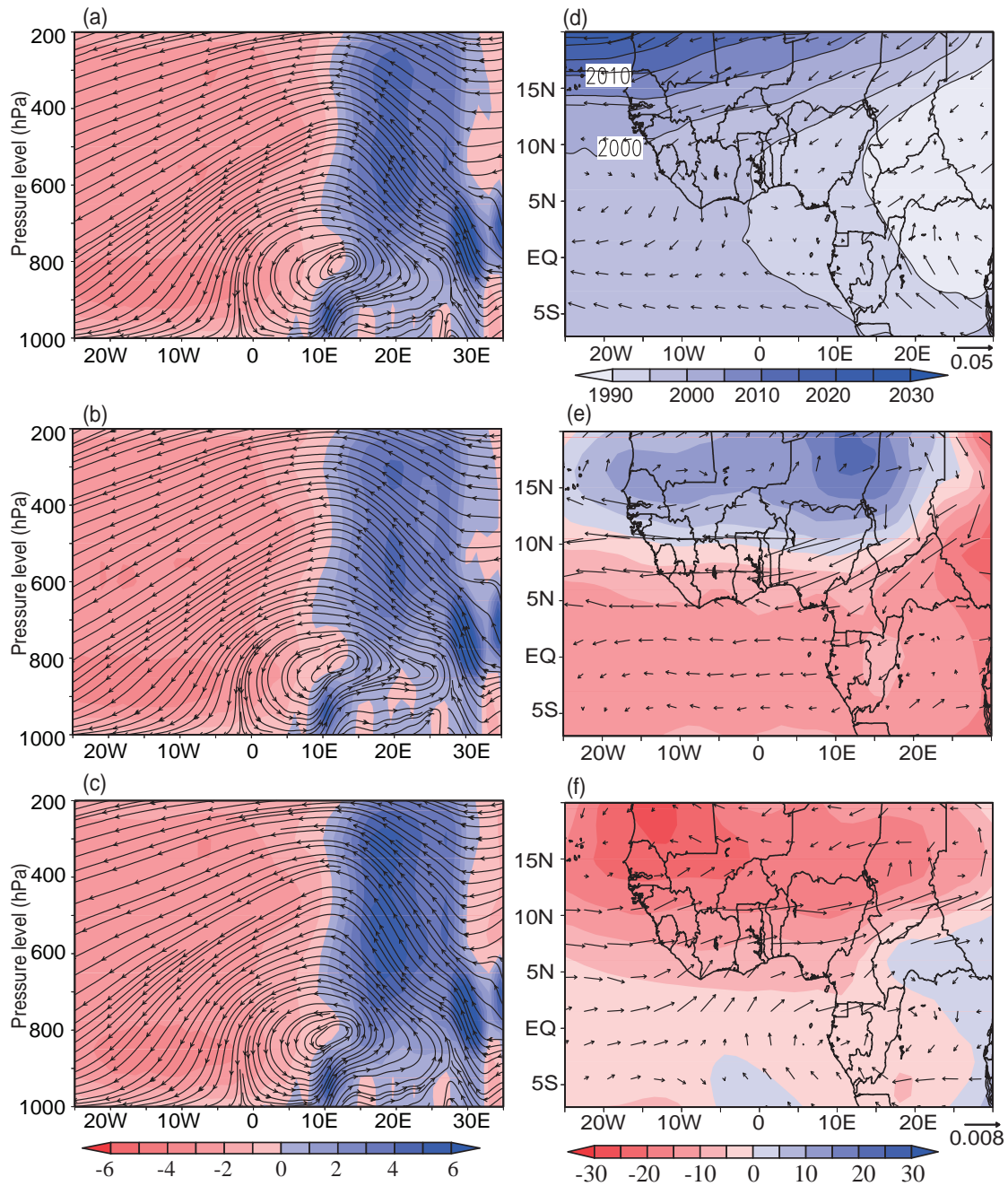
Fig. 11. ERA-Interim longitude–height cross section of streamlines [u (m s^{-1}); $-\omega \times 10^2$ (Pa s^{-1})] and vertical winds ($\times 10^2$ Pa s^{-1}; shaded), averaged over 5°S–3°N from the (a) JAS climatology, and the (b) weak and (c) strong Congo basin Walker circulation composites. Blue coloring indicates upward vertical motion. (d) ERA-Interim JAS climatological 800-hPa moisture transport ($q.\boldsymbol{u}$; vectors) and geopotential heights (shaded). (e) Moisture transport and geopotential height differences in the weak composite and the climatology. (f) As in (e) but for the strong composite. Units for geopotential height and moisture transport are gpm and kg kg^{-1} m s^{-1}.

are up to -1.5 gpm lower over the Gulf and the Congo basin (Fig. 11e). Associated with these height differences, easterly and northeasterly moisture transport anomalies develop over the Congo basin and the Sahel. Also, with weakening of the west African westerly jet (Pu and Cook, 2010), westerly moisture transport from the West African coast to the central Sahel lowers, as shown by the easterly moisture transport anomalies around 11°N, and the moisture level reduces in the

central Sahel (not shown). In contrast, there is a general reduction, up to -2.5 gpm, of height over the Sahel and the Congo basin ($\sim$5°S, 18°E) in the strong composite. This is associated with increases in moisture transport, as indicated by the westerly and southwesterly anomalies over the western coast of West Africa and the Gulf (Fig. 11f). As the zonal circulation becomes stronger, surface to 800-hPa moisture increases in the Sahel and coastal inland areas within (2°–7°N,

0°–20°E) (not shown). As discussed in Lélé et al. (2015), the low-level flows—especially below 850 hPa—constitute an important source of moisture supplying the West African monsoon system. This means that when the rising branch of the circulation is anomalously strong, the Congo basin and Sahelian moisture transports become strong.

The JAS cloud cover in ERA-Interim matches fairly well with ISCCP (1983–2009) observations (not shown). Most of the cloud in ERA-Interim over the analysis region is low cloud (~70%, below 800 hPa). Changes in the low-cloud cover are examined. The JAS mean low-cloud cover differences displayed in Fig. 12a are for the weak composite and climatology, while Fig. 12b shows the results for the strong composite and climatology. The cloud over land, including over the Sahel and the Congo basin, and along the coastal upwelling region to the south of the equator, reduces, up to −6%, in the weak composite (Fig. 12a). Meanwhile, the cloud cover increases, up to 4%, over the northern Guinean Gulf, resulting in lower amounts of solar flux to the surface. In contrast to the weak composite, the cloud amounts in the strong composite increase generally over land but decrease over the ocean (Fig. 12b). An enhancement, up to 12%, occurs over the Congo basin and Sahel, permitting relatively smaller amounts of solar radiation. Over the Gulf of Guinea, cloud amounts lower, up to −8%, allowing more incoming solar radiation to heat up the surface (not shown).

Figure 12c displays the differences in OLR in the weak composite and climatology (from the NOAA OLR), while the differences in the strong composite and climatology are displayed in Fig. 12d. Changes in cloud cover in ERA-Interim are consistent with the NOAA OLR. Associated with the decreased cloud cover over the Sahel and the Congo basin, the OLR value is, up to 10 W m^{-2}, greater in the weak composite than in the climatology (Figs. 12a and c). Also, associated with the increased cloud cover, reductions, up to −6 W m^{-2}, occur in the strong composite (Figs. 12b and d).

The difference between the weak and strong composites is largely due to land surface heating. Associated with weak rising motion over the Congo basin, cloud cover reduces, allowing larger amounts of incoming solar radiation to increase the surface temperature in the weak composite. In contrast, cloud amounts increase generally over land, reducing the amount of incoming solar heat flux, and this cools the surface in the strong composite.

Figure 12e displays the PERSIANN-CDR JAS precipitation differences in the weak composite and climatology, while the differences in the strong composite and climatology are displayed in Fig. 12f. Associated with the weakening of the Congo basin circulation, rainfall reduces, by up to −2.5 mm d^{-1}, in the central Sahel, southern Chad. In contrast, as the circulation becomes strong, rainfall rates enhance, by up to 2.5 mm d^{-1} in the central Sahel and the Congo basin. Also, rainfall rates increase, by up to 2 mm d^{-1}, over the west coast of Africa in the strong composite, while reductions occur in the weak composite. Investigating the causes of these differences is beyond the scope of the present study.

In summary, the Congo basin zonal overturning circulation is tightly connected with the West African monsoon system. A strong circulation is associated with increased subsidence over the Gulf of Guinea, and this supports greater northward moisture transport and increases of precipitation in the Sahel (Figs. 11 and 12f).

4. Conclusions

This paper comprehensively documents the Gulf of Guinea subsidence and identifies a Congo basin zonal overturning circulation, whose down branch is associated with the presence of this subsidence. The interannual variability of the circulation and its relationship with moisture and precipitation distributions across West Africa are explored.

The Guinean subsidence develops in the low levels at the beginning of June, attains a maximum intensity of 6×10^{-2} Pa s^{-1}, reaching as far as 5°N during boreal summer (JAS), and dissipates in October. This subsidence is associated with a complete zonal circulation, which has the same seasonality as that of the Guinean subsidence in ERA-Interim, ERA-40, NCEP-2 and MERRA. The circulation is identified as a Congo basin zonal overturning circulation. The circulation comprises of: (1) a low-level westerly flow from the Gulf to the Congo basin (lower branch); (2) rising winds over the basin around 20°E (up-branch); (3) easterly return flow from the basin to the Gulf of Guinea at 600 hPa (upper branch); and (4) subsiding winds over the Gulf centered around 2°W (down-branch)—with winds to the east flowing eastward to complete the circulation. This circulation reaches its maximum intensity in the summer from July to September.

Analysis of the momentum budget shows that the low-level flow is strongly ageostrophic, with a small acceleration term and Coriolis term, which is zero at the equator, and large pressure gradient and friction terms. The eastward-directed pressure gradient force drives the flow from the Gulf of Guinea toward the Congo basin, constituting the lower branch of the zonal overturning circulation. The pressure gradient term is larger over the Congo basin than over the Gulf of Guinea. Over the basin, it is comparable to the residual term, which opposes the wind direction. The residual is interpreted as friction, and is expected to be much larger over land with complex topography. Associated with this friction, winds converge and rise over the Congo basin forming the up-branch of the circulation. Causes of the pressure gradient force are explored.

Analysis of surface temperature explains the eastward decreasing pressure gradient force that drives the circulation and much of its seasonal variation. Temperature is (in ERA-Interim, for example) up to −5 K lower in the Gulf of Guinea than in the Congo basin, and, associated with this gradient, the surface pressure is lower over land than over the ocean.

The differences in the Gulf of Guinea–Congo basin temperatures are primarily caused by differences in the land temperatures, which are model-dependent, in the reanalyses. Land temperature and precipitation in ERA-40, NCEP-2 and MERRA are much warmer and drier than in the observations. ERA-Interim is selected to understand the variability of the
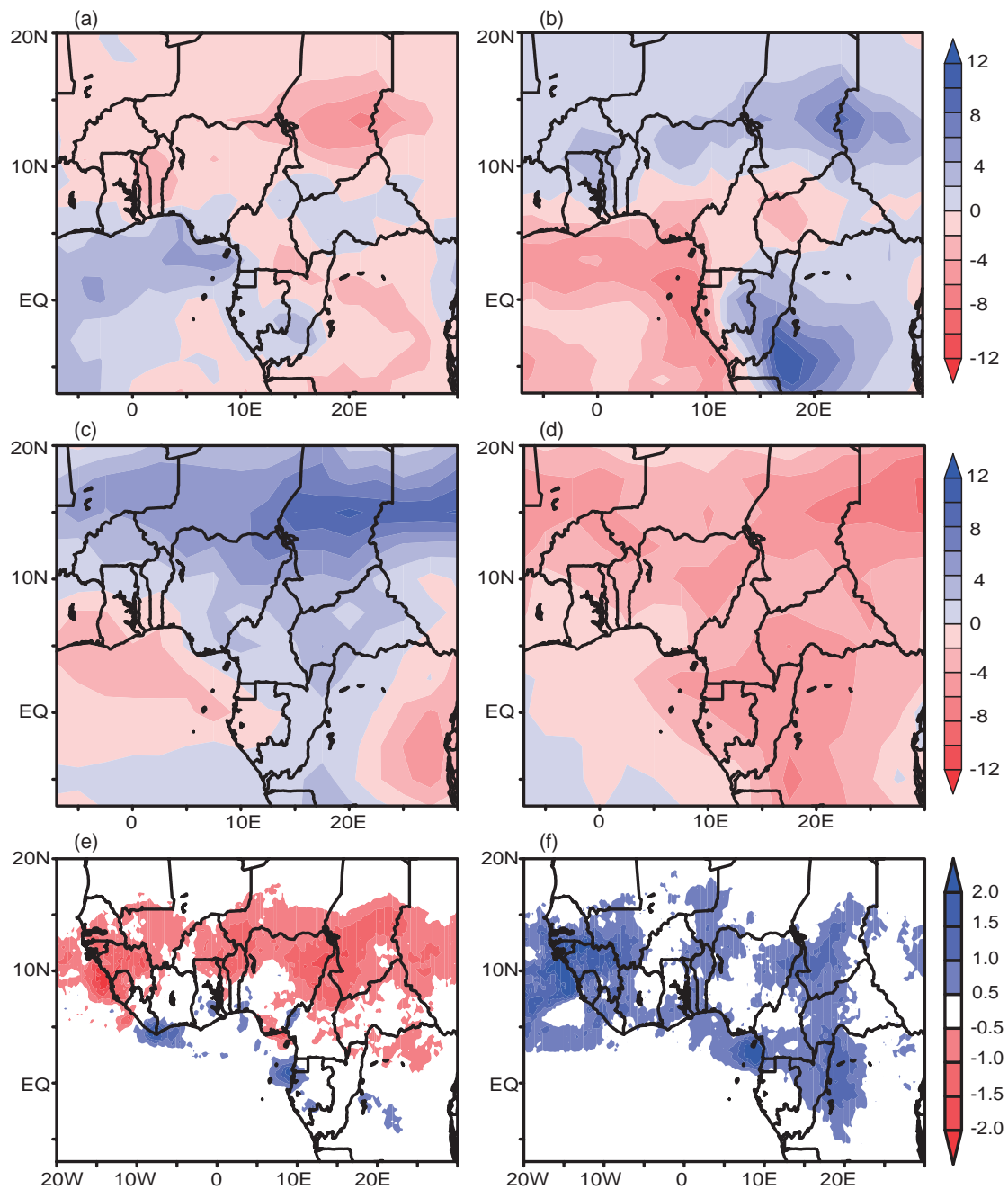
Fig. 12. (a) Low-cloud cover (%) differences in the weak composite and the JAS mean from the ERA-Interim climatology. (b) As in (a) but for the strong composite. (c) OLR (W m^{-2}) differences in the weak composite and the JAS mean from the NOAA climatology. (d) As in (c) but for the strong composite. (e) Precipitation (mm d^{-1}) differences in the weak composite and the JAS mean from the PERSIANN-CDR climatology. (f) As in (e) but for the strong composite. Contour interval is every 2% in (a, b) and 2 W m^{-2} in (c, d).

circulation based on its realistic representation of temperature and precipitation.

Correlation between the Congo basin p-velocity index and the low-level vertical velocity field on interannual timescales reveals that the Congo basin rising motion is significantly correlated, up to -0.5, with the Guinean subsidence in ERA-Interim. Based upon the strength of the up-branch, two composites are created to explore the relation-

ship between the equatorial overturning circulation and regional circulation and rainfall over the Sahel. Examination of the low-level flows shows that the Congo basin circulation is related to moisture distributions across West Africa and the Congo basin. Along with the weakening of the circulation, the Guinean subsidence becomes weak. This supports the development of convection over the Gulf of Guinea, and northward moisture transport and precipitation over the Sa-

hel reduces. In contrast, when the circulation is stronger, the Guinean subsidence becomes stronger, and this inhibits convection over the Gulf of Guinea, supporting northward and eastward moisture transport associated with enhancements of precipitation over the Sahel and the Congo basin.

Having established the important role of the Congo basin zonal overturning circulation in moisture and precipitation distributions across West Africa and the Congo basin in observations, further investigation of the circulation in the state-of-the-art climate models will be addressed in a subsequent paper.

REFERENCES

Caniaux, G., H. Giordani, J.-L. Redelsperger, F. Guichard, E. Key, and M. Wade, 2011: Coupling between the Atlantic cold tongue and the West African monsoon in boreal spring and summer. *J. Geophys. Res.*, **116**, C04003, doi: 10.1029/2010 JC006570.

Cook, K. H., and E. K. Vizy, 2006: Coupled model simulations of the West African monsoon system: Twentieth-and twenty-first-century simulations. *J. Climate*, **19**, 3681–3703.

Cook, K. H., and E. K. Vizy, 2015: The Congo Basin walker circulation: Dynamics and connections to precipitation. *Climate Dyn.*, 1–21, doi: 10.1007/s00382-015-2864-y.

Dee, D. P., and S. Uppala, 2009: Variational bias correction of satellite radiance data in the ERA-Interim reanalysis. *Quart. J. Roy. Meteor. Soc.*, **135**, 1830–1841.

Dee, D. P., and Coauthors, 2011: The ERA-Interim reanalysis: Configuration and performance of the data assimilation system. *Quart. J. Roy. Meteor. Soc.*, **137**, 553–597.

Dezfuli, A. K., and S. E. Nicholson, 2013: The relationship of rainfall variability in western equatorial Africa to the tropical Oceans and atmospheric circulation. Part II: The boreal autumn. *J. Climate*, **26**(1), 66–84, doi: 10.1175/JCLI-D-11-00686.1.

Dezfuli, A. K., B. F. Zaitchik, and A. Gnanadesikan, 2015: Regional Atmospheric circulation and rainfall variability in south equatorial Africa. *J. Climate*, **28**(2), 809–818, doi: 10.1175/JCLI-D-14-00333.1.

Fontaine, B., P. Roucou, and S. Trzaska, 2003: Atmospheric water cycle and moisture fluxes in the West African monsoon: mean annual cycles and relationship using NCEP/NCAR reanalysis. *Geophys. Res. Lett.*, **30**, 1117, doi: 10.1029/2002GL 015834.

Grist, J. P., and S. E. Nicholson, 2001: A study of the dynamic factors influencing the rainfall variability in the west African Sahel. *J. Climate*, **14**, 1337–1359.

Hagos, S. M., and K. H. Cook, 2007: Dynamics of the West African monsoon jump. *J. Climate*, **20**, 5264–5284.

Hagos, S. M., and C. D. Zhang, 2010: Diabatic heating, divergent circulation and moisture transport in the African monsoon system. *Quart. J. Roy. Meteor. Soc.*, **136**, 411–425.

Hastenrath, S., 2001: In search of zonal circulations in the equatorial Atlantic sector from the NCEP-NCAR reanalysis. *Int. J. Climatol.*, **21**, 37–47.

Hastenrath, S., 2006: Circulation and teleconnection mechanisms of northeast Brazil droughts. *Prog. Oceanogr.*, **70**, 407–415.

Hastenrath, S., and P. J. Lamb, 2004: Climate dynamics of atmosphere and ocean in the equatorial zone: A synthesis. *Int. J Climatol.*, **24**, 1601–1612.

Hastenrath, S., and D. Polzin, 2011: Long-term variations of circulation in the tropical Atlantic sector and Sahel rainfall. *Int. J. Climatol*, **31**, 649–655.

Kanamitsu M., W. Ebisuzaki, J. Woollen, S. K. Yang, J. J. Hnilo, M. Fiorino, and G. L. Potter, 2002: NCEP-DOE AMIP-II Reanalysis (R-2). *Bull. Amer. Meteor. Soc.*, **83**, 1631–1643.

Kobayashi, S., M. Matricardi, D. Dee, and S. Uppala, 2009: Toward a consistent reanalysis of the upper stratosphere based on radiance measurements from SSU and AMSU-A. *Quart. J. Roy. Meteor. Soc.*, **135**, 2086–2099.

Kummerow, C., W. Barnes, T. Kozu, J. Shiue, and J. Simpson, 1998: The Tropical Rainfall Measuring Mission (TRMM) sensor package. *J. Atmos. Oceanic Technol.*, **15**, 809–817.

Lau, K.-M., and S. Yang, 2003: Walker circulation. *Encyclopedia of Atmospheric Sciences*, J. R. Holton et al., Eds., Academic Press, 2505–2510.

Leduc-Leballeur, M., G. de Coëtlogon, and L. Eymard, 2013: Air–Sea interaction in the Gulf of Guinea at intraseasonal time-scales: Wind bursts and coastal precipitation in boreal spring. *Quart. J. Roy. Meteor. Soc.*, **139**, 387–400, doi: 10.1002/qj. 1981.

Lélé, M. I., L. M. Leslie, and P. J. Lamb, 2015: Analysis of low-level atmospheric moisture transport associated with the West African monsoon. *J. Climate*, **28**, 4414–4430, doi: 10.1175/JCLI-D-14-00746.1.

Liebmann, B., and C. A. Smith, 1996: Description of a complete (interpolated) outgoing longwave radiation dataset. *Bull. Amer. Meteor. Soc.*, **77**, 1725–1277.

Mitchell, T. D., and P. D. Jones, 2005: An improved method of constructing a database of monthly climate observations and associated high-resolution grids. *Int. J. Climatol.*, **25**, 693–712, doi: 10.1002/joc.1181.

Neupane, N., and K. H. Cook, 2013: A nonlinear response of Sahel rainfall to Atlantic warming. *J. Climate*, **26**, 7080–7096, doi: 10.1175/JCLI-D-12-00475.1.

Nicholson, S. E., and P. J. Webster, 2007: A physical basis for the interannual variability of rainfall in the Sahel. *Quart. J. Roy. Meteor. Soc.*, **133**, 2065–2084.

Nicholson, S. E., and A. K. Dezfuli, 2013: The relationship of rainfall variability in western equatorial Africa to the tropical Oceans and atmospheric circulation. Part I: The boreal spring. *J. Climate*, **26**(1), 45–65, doi: 10.1175/JCLI-D-11-00653.1.

Nolan, D. S., C. D. Zhang, and S. H. Chen, 2007: Dynamics of the shallow meridional circulation around intertropical convergence zones. *J. Atmos. Sci.*, **64**, 2262–2285.

Pokam, W. M., L. A. T. Djiotang, and F. K. Mkankam, 2012: At-

mospheric water vapor transport and recycling in equatorial central Africa through NCEP/NCAR reanalysis data. *Climate Dyn.*, **38**(9–10), 1715–1729, doi: 10.1007/s00382-011-1242-7.

Pokam, W. M., C. L. Bain, R. S. Chadwick, R. Graham, D. J. Sonwa, and F. M. Kamga, 2014: Identification of processes driving low-level westerlies in west equatorial Africa. *J. Climate*, **27**(11), 4245–4262, doi: 10.1175/JCLI-D-13-00490.1.

Pu, B., and K. H. Cook, 2010: Dynamics of the West African westerly jet. *J. Climate*, **23**(23), 6263–6276.

Rienecker, M. M., and Coauthors, 2011: MERRA: NASA's modern-era retrospective analysis for research and applications. *J. Climate*, **24**, 3624–3648.

Segele, Z.T., P. J. Lamb, and L. M. Leslie, 2009: Large-scale atmospheric circulation and global sea surface temperature associations with Horn of Africa June–September rainfall. *Int. J. Climatol.*, **29**(8), 1075–1100.

Simmons, A., S. Uppala, D. Dee, and S. Kobayashi, 2007: ERA-Interim: New ECMWF Reanalysis Products from 1989 Onwards. ECMWF Newsletter, No.110, ECMWF, Reading, United Kingdom, 25–35.

Simmons, A.J., K. M. Willett, P. D. Jones, P. W. Thorne, and D. P. Dee, 2010: Low-frequency variations in surface atmospheric humidity, temperature, and precipitation: Inferences from reanalyses and monthly gridded observational data sets. *Journal of Geophysical Research: Atmospheres (1984–2012)*, **115**, D01110, doi:10.1029/2009JD012442.

Sorooshian, S., K.-L. Hsu, X. G. Gao, H. V. Gupta, B. Imam, and D. Braithwaite, 2000: Evaluation of PERSIANN system satellite-based estimates of tropical rainfall. *Bull. Amer. Meteor. Soc.*, **81**, 2035–2046.

Thorncroft, C. D., and M. Blackburn, 1999: Maintenance of the African easterly jet. *Quart. J. Roy. Meteor. Soc.*, **125**, 763–786.

Thorncroft, C. D., H. Nguyen, C. D. Zhang, and P. Peyrillé, 2011: Annual cycle of the West African monsoon: Regional circulations and associated water vapour transport. *Quart. J. Roy. Meteor. Soc.*, **137**, 129–147.

Trenberth, K. E., D. P. Stepaniak, and J. M. Caron, 2000: The global monsoon as seen through the divergent atmospheric circulation. *J. Climate*, **13**, 3969–3993.

Uppala, S. M., and Coauthors, 2005: The ERA-40 re-analysis. *Quart. J. Roy. Meteor. Soc.*, **131**, 2961–3012.

Uppala, S. M., D. P. Dee, S. Kobayashi, P. Berrisford, and A. J. Simmons, 2008: Towards a climate data assimilation system: status update of ERA-Interim. ECMWF Newsletter, No. 115, ECMWF, Reading, United Kingdom, 12–18.

Vizy, E. K., and K. H. Cook, 2001: Mechanisms by which Gulf of Guinea and eastern North Atlantic Sea surface temperature anomalies can influence African rainfall. *J. Climate*, **14**, 795–821.

Wang, C., 2005: ENSO, Atlantic climate variability, and the Walker and Hadley circulations. *The Hadley Circulation: Present, Past, and Future*, H. F. Diaz and R. S. Bradley, Eds., Kluwer Academic Publishers, 173–202.

Wang, C. Z., 2002a: Atlantic climate variability and its associated atmospheric circulation cells. *J. Climate*, **15**, 1516–1536.

Wang, C. Z., 2002b: Atmospheric circulation cells associated with the El Niño–southern oscillation. *J. Climate*, **15**, 399–419.

Wang, C. Z., 2004: ENSO, Atlantic climate variability, and the Walker and Hadley circulations. *The Hadley Circulation: Present, Past, and Future*, H. F. Diaz and R. S. Bradley, Eds., Advances in Global Change Research, Vol. 21, Springer, Netherlands, 85–120.

Washington, R., R. James, H. Pearce, W. M. Pokam, and W. Moufouma-Okia, 2013: Congo Basin rainfall climatology: can we believe the climate models? *Philosophical Transactions of the Royal Society of London. Series B, Biological Sciences*, **368**(1625), 20120296, doi: 10.1098/rstb.2012.0296.

Zhang, C. D., P. Woodworth, and G. J. Gu, 2006: The seasonal cycle in the lower troposphere over West Africa from sounding observations. *Quart. J. Roy. Meteor. Soc.*, **132**, 2559–2582.